Global Biogeochemical Cycles

RESEARCH ARTICLE
10.1029/2020GB006718

Key Points:

- Global oceanic gross primary production (GPP) of 103 ~ 150 Pg C yr^{-1} is estimated by machine learning algorithms trained on two datasets
- GPP estimated by the triple isotopes of dissolved oxygen is higher than that measured by the light-dark bottle incubation by a factor of 1.6
- Oceanic GPP is 1.5–2.2 times greater than NPP and comparable to the GPP on land

Supporting Information:

- Supporting Information S1

Correspondence to:
N. Cassar,
Nicolas.Cassar@duke.edu

Citation:
Huang, Y., Nicholson, D., Huang, B., & Cassar, N. (2021). Global estimates of marine gross primary production based on machine learning upscaling of field observations. *Global Biogeochemical Cycles*, *35*, e2020GB006718. https://doi.org/10.1029/2020GB006718

Received 20 JUN 2020
Accepted 7 JAN 2021

Global Estimates of Marine Gross Primary Production Based on Machine Learning Upscaling of Field Observations

Yibin Huang[1,3,4], David Nicholson[2], Bangqin Huang[3,4], and Nicolas Cassar[1,5]

[1]Division of Earth and Ocean Sciences, Nicholas School of the Environment, Duke University, Durham, NC, USA, [2]Department of Marine Chemistry and Geochemistry, Woods Hole Oceanographic Institution, Woods Hole, MA, USA, [3]State Key Laboratory of Marine Environmental Science, Xiamen University, Xiamen, China, [4]Fujian Provincial Key Laboratory of Coastal Ecology and Environmental Studies, Xiamen University, Xiamen, China, [5]Laboratoire des Sciences de l'Environnement Marin (LEMAR), Institut Universitaire Européen de la Mer (IUEM), Brest, France

Abstract Approximately half of global primary production occurs in the ocean. While the large-scale variability in net primary production (NPP) has been extensively studied, ocean gross primary production (GPP) has thus far received less attention. In this study, we derived two satellite-based GPP models by training machine learning algorithms (Random Forest) with light-dark bottle incubations (GPP_{LD}) and the triple isotopes of dissolved oxygen ($GPP_{17\Delta}$). The two algorithms predict global GPPs of $9.2 \pm 1.3 \times 10^{15}$ and $15.1 \pm 1.05 \times 10^{15}$ mol O_2 yr^{-1} for GPP_{LD} and $GPP_{17\Delta}$, respectively. The projected GPP distributions agree with our understanding of the mechanisms regulating primary production. Global $GPP_{17\Delta}$ was higher than GPP_{LD} by an average factor of 1.6 which varied meridionally. The discrepancy between $GPP_{17\Delta}$ and GPP_{LD} simulations can be partly explained by the known biases of each methodology. After accounting for some of these biases, the $GPP_{17\Delta}$ and GPP_{LD} converge to $9.5 \sim 12.6 \times 10^{15}$ mol O_2 yr^{-1}, equivalent to 103 ~ 150 Pg C yr^{-1}. Our results suggest that global oceanic GPP is 1.5–2.2 fold larger than oceanic NPP and comparable to GPP on land.

1. Introduction

Photosynthesis is one of the central biological processes on Earth. It is the main source of organic matter to ecosystems and modulates cycles of carbon, nutrients and water, thereby influencing the global climate. Therefore, accurate quantification of photosynthesis is critical for understanding ecosystem functions and predicting the feedbacks between the biosphere and climate.

Two fluxes relevant to photosynthesis are gross primary production (GPP) and net primary production (NPP). In the literature, GPP refers to the total amount of oxygen production associated with the splitting of water at photosystem II (PSII; Juranek & Quay, 2013; Quay et al., 2010) and excluding autotrophic respiration (Chavez et al., 2011; Sigman and Hain, 2012). NPP, defined as GPP minus the carbon lost by autotrophic respiration (AR), represents the organic carbon available for heterotrophic activity, accumulation, and export (Equation 1).

$$CO_2 + H_2O \xrightarrow[\underbrace{\text{Photosynthesis}}_{\text{GPP}}]{\overbrace{\phantom{\text{Photosynthesis}}}^{\text{NPP}}\ \overbrace{\phantom{\text{AR}}}^{\text{AR}}} \text{Organic matter} + O_2 \quad (1)$$

In ocean ecosystems, primary production can be estimated by various approaches generally classified into two types: incubation-based and geochemical (incubation-independent) approaches. The former approaches mainly include the ^{14}C-inorganic carbon incorporation methods (Steemann Nielsen, 1952), oxygen evolution between light-dark bottles (Serret et al., 1999), the $H_2{}^{18}O$-labeling approach (M. Bender et al., 1987) and nutrient uptake experiments (Dugdale & Goering, 1967). The incubation-independent approaches are generally based on geochemical tracers of productivity, including the triple isotopes of dissolved oxygen (Luz & Barkan, 2000), analysis of oxygen records from moorings and gliders (Nicholson 2008, Nicholson et al., 2014) and electron transport measurements by active fluorescence (Kolber et al., 1998). Among the

approaches, the ^{14}C-inorganic carbon incorporation technique has traditionally been the most commonly used method and has generated a large global dataset over the past 60 years (Chavez et al., 2011; Peterson, 1980). The ^{14}C-based approach measures GPP, NPP or net community production depending, among other things, on the incubation duration (Dring et al., 1982; Marra, 2009). Additionally, the dissolved organic carbon excreted by phytoplankton or by zooplankton (Carlson & Hansell, 2015; Laws et al., 2000; Myklestad, 2000; Teira et al., 2001) is traditionally not accounted for when measuring ^{14}C on GF/F filters (size fraction of 0.7 *u*m or larger). In contrast, the oxygen-based methods generally account for both particulate and dissolved organic carbon production, thereby providing estimates closer to GPP (González et al., 2008). In light-dark bottle incubations, GPP is estimated from the sum of O_2 evolution in the dark (i.e., community respiration) and in the light (i.e., net community production). In the $H_2{}^{18}O$-labeling approach, a negligible fraction of the photosynthetically-evolved $^{18}O_2$ is recycled because it is diluted in the large dissolved O_2 pool (M. Bender et al., 1987; Juranek & Quay, 2005). In the triple isotopes of dissolved oxygen approach, combining natural $^{18}\delta$ and $^{17}\delta$ signatures removes the mass dependent fractionation associated with respiration to calculate the relative contribution of photosynthetic and atmospheric end-members to the isotopic signature of O_2 at the ocean surface (Lämmerzahl et al., 2002; Luz & Barkan, 2000).

Satellite-based remote sensing and biogeochemical models have broadened our understanding of the temporal and spatial variability in oceanic primary production (Behrenfeld & Falkowski, 1997; Friedrichs et al., 2009; Letscher & Moore, 2017; Westberry et al., 2008). Among these, VPGM and CbPM are two of the most widely used satellite-based models. These two models are semi-mechanistic and semi-empirical, hybrid in nature between mechanistic and statistical models. For example, the three light dependent terms in VGPM were parameterized using the MARMAP Dataset (Behrenfeld & Falkowski, 1997). 97% of measurements in this dataset were based on ^{14}C incubations which are longer than 6h. The most critical photosynthesis parameters (P_b^{opt}) was parameterized with *in situ* measurements of sea surface temperature and field ^{14}C observation (Behrenfeld & Falkowski, 1997). Although the CbPM model didn't directly integrate ^{14}C-based measurements in the model construction, comparisons with field observations at two time-series stations (HOT and BATS) suggest the model is consistent with 24h ^{14}C-based productivity estimates (Westberry et al., 2008). Therefore, the global map derived from these two algorithms can be viewed as NPP. These models estimate a global marine NPP of 44–67 Pg C yr^{-1}, similar to that on land (60 Pg C yr^{-1}; Field et al., 1998; Zhao & Running, 2010). Terrestrial GPP and NPP have been well studied with the former being on the order of 112–148 Pg C yr^{-1} (Anav et al., 2015; Beer et al., 2010; Waring et al., 1998). In contrast, studies of marine GPP are generally limited to local and regional scales (Quay et al., 2010; Serret et al., 2015). Recently, Carvalho et al. (2017) inferred a range of global oceanic GPP between 70 and 145 Pg C yr^{-1} based on global NPP and an empirically derived fraction of autotrophic respiration loss. The lack of independent estimates of global marine GPP limits our understanding of marine primary production, the metabolic demands of autotrophs and their role in the global carbon cycle.

Strategies to model the broad distribution of oceanic properties can be classified into two types. The first is process based, relying on mechanistic or biogeochemical models (Moore et al., 2013; Siegel et al., 2014). Such an approach can provide unique insight into the underlying mechanisms. However, accurate representation (and/or parameterization) of complex and sometimes poorly understood processes is a challenge. The second strategy is data-driven. While such an approach does not directly provide insight into the mechanisms, it can be used to model the distribution of a property and in some cases provide some quantitative intuition into the underlying processes through statistical inferences. Among these methods, machine learning approaches have gained popularity, being applied to estimate the global distribution of various ocean properties such as zooplankton biomass (Mazzocchi et al., 2014), seafloor organic carbon (T. R. Lee et al., 2019), net community production (Li & Cassar, 2016) and N_2 fixation (Tang et al., 2019).

In this study, we present a first attempt at estimating global GPP by training machine learning algorithms with two meta-analyzed datasets. The first dataset is based on O_2 evolution during light and dark bottle incubations (GPP_{LD}; Serret et al., 1999). The second is based on *in situ* estimates of the triple isotopes of dissolved oxygen ($GPP_{17\Delta}$; Luz & Barkan, 2000). Taking advantage of machine learning techniques, we constructed data-driven algorithms based on the two datasets to estimate GPP for the global ocean. This novel approach advances our understanding of marine carbon cycling and can be used to validate process-based models.

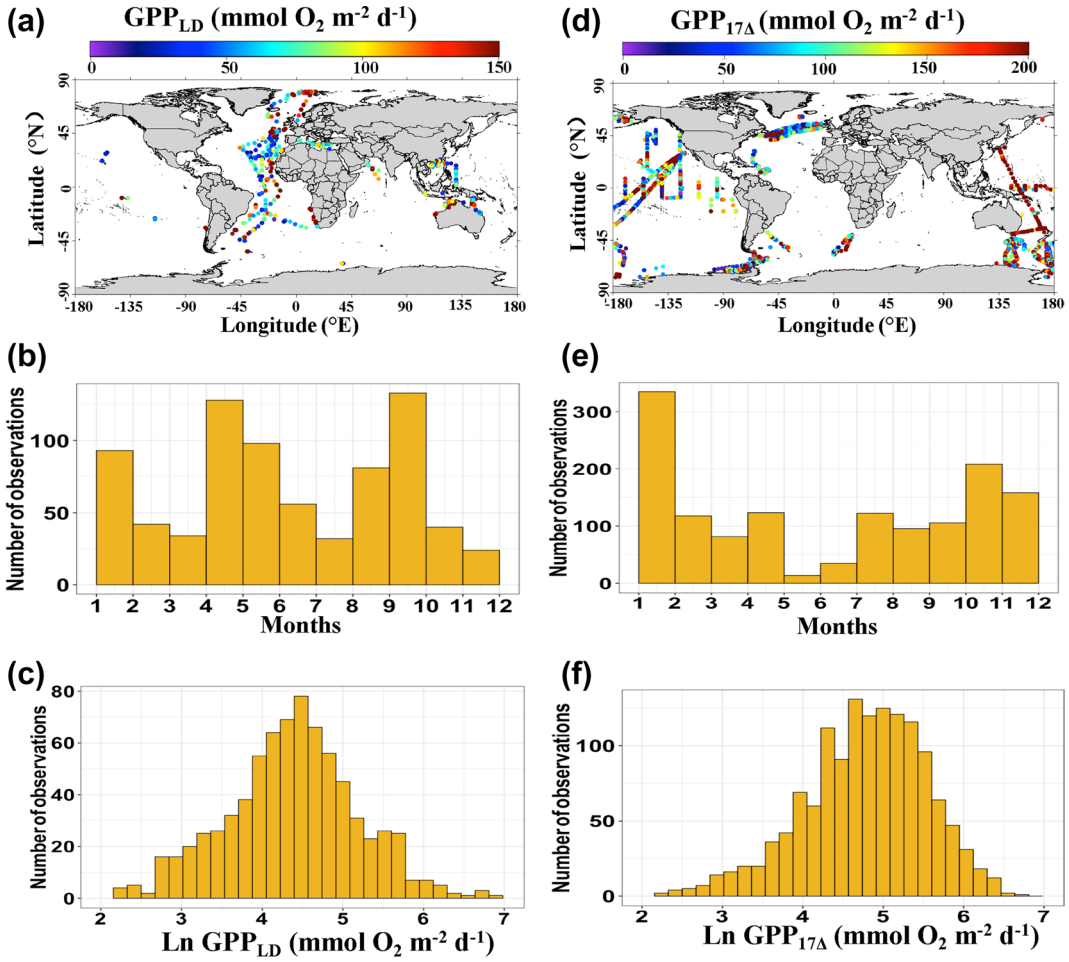

Figure 1. The locations and distributions of gross primary production (GPP) estimates derived from (a) oxygen evolution during light-dark bottle incubations (GPP_{LD}) (b) triple isotopes of dissolved oxygen ($GPP_{17\Delta}$). The bottom histograms show the frequency distributions of the sampling month and GPP estimates.

2. Methods

2.1. Meta-Analysis of Global GPP

2.1.1. GPP Derived from the Diel Oxygen Changes in Light-Dark Bottle Incubations

To train and validate our machine learning algorithms, we compiled a global dataset of GPP derived from light-dark bottle incubations (Figure 1, Table S1). The light-dark bottle method has been used to assess primary production for nearly a century (Gaarder & Gran, 1927). GPP is estimated from the photosynthetic evolution of oxygen in the light incubation with a correction for respiratory O_2 consumption in the dark incubation (typically 24 h; Serret et al., 1999). The method relies on the assumption that daytime and nighttime respiration are equivalent. In our study, volumetric primary production observations were depth-integrated over the euphotic zone using the trapezoidal integration method. We did not incorporate GPP estimates derived from $H_2{}^{18}O$-label incubations (M. Bender et al., 1987) into our training dataset as discrepancies between the two incubation approaches might introduce uncertainties in the predictions. GPP estimates derived from $H_2{}^{18}O$-label are also too sparse to reliably train the algorithms.

2.1.2. GPP Derived from the Triple Isotopes of Dissolved Oxygen

We also compiled a dataset of GPP estimates based on the *in situ* measurement of the triple isotopes of dissolved oxygen ($^{18}\delta$, $^{17}\delta$ and $^{16}\delta$, Table S1). This approach is increasingly being used to constrain marine productivity (Juranek & Quay, 2013; Luz & Barkan, 2000). Oceanic oxygen originates from atmospheric

gas exchange and photosynthetic evolution. Atmosphere-derived dissolved oxygen has a known mass independent depletion of $^{17}\delta$ relative to $^{18}\delta$ resulting from a stratospheric reaction (Lämmerzahl et al., 2002; Luz & Barkan, 2000), whereas photosynthetic O_2 derived from seawater has high $^{17}\delta$, resulting in excess $^{17}\delta$ relative to the atmospherically derived oxygen. Respiration alters the $^{18}\delta$ and $^{17}\delta$ signals in a known mass-dependent manner. Thus, the observed mass-independent anomaly in the $^{18}\delta$ and $^{17}\delta$ isotopic ratios observed in the surface ocean O_2 reflects the relative proportion of O_2 derived from photosynthesis versus air-sea gas exchange. Assuming steady-state and parameterizing the gas exchange rate, the integrated GPP within the mixed-layer can be approximated using the "dual delta" approach recommended by Kaiser (2011) and Prokopenko et al. (2011):

$$\frac{GPP}{k_{O_2}O_{eq}} = \frac{\left(1-\frac{10^{-317}\delta O_{eq}+1}{10^{-317}\delta O_{dis}+1}\right)-\lambda\left(1-\frac{10^{-318}\delta O_{eq}+1}{10^{-318}\delta O_{dis}+1}\right)}{\left(\frac{10^{-317}\delta O_{p}+1}{10^{-317}\delta O_{dis}+1}-1\right)-\lambda\left(\frac{10^{-318}\delta O_{P}+1}{10^{-318}\delta O_{dis}+1}-1\right)} \quad (2)$$

The subscripts *dis*, *eq* and *p* stand for dissolved, equilibrium and photosynthetic, respectively. We assigned 0.411‰ for $^{17}\delta O_{eq}$, −0.779‰ for $^{18}\delta O_{eq}$, and −11.902‰ for $^{17}\delta O_p$ (Kaiser, 2011; Prokopenko et al., 2011). λ is the empirically derived slope for mass-dependent respiration fractionation equal to 0.518 (Helman et al., 2005; Luz & Barkan, 2005). O_{eq} is the oxygen concentration at saturation calculated with seawater temperature and salinity (Garcia & Gordon, 1992). k_{O_2} represents the air-sea gas exchange velocity for oxygen. We calculated k_{O_2} using QSCAT/NCEP blended wind speeds (Colorado Research Associates/Northwest Research Associates/Inc., 2001), monthly climatological mixed layer depth (MLD; Hosoda et al., 2010) and the gas exchange parameterization of Wanninkhof (2014). A weighted technique (Reuer et al., 2007, Teeter et al., 2018) is adopted to account for the effect of wind speed history (60 days before the sampling days) on k_{O_2} (Supporting Information). Our $GPP_{17\Delta}$ estimates carry both random and systemic errors. The assumptions of steady-state and negligible role of lateral advection and vertical entrainment are violated under some conditions (Hamme et al., 2012; Nicholson et al., 2014). There are also uncertainties introduced with errors in end-members (Kaiser, 2011) and the mass dependent fractionation associated with respiratory O_2 consumption (Ash et al., 2020). A recent experiment conducted in freshwater challenges the empirical respiratory isotopic fractionation of 0.518, suggesting an upward revision to 0.522 (Ash et al., 2020). These results warrant further study in marine environments. The wind speed parameterization of the gas exchange velocity also introduces errors in our estimates of approximately ±30% (M. L. Bender et al., 2011; Emerson et al., 2019). As there are no absolute GPP standards, the only approach is to compare independent methods (M. Bender et al., 1999; Quay et al., 2010; Regaudie-de-Gioux et al., 2014).

2.2. Matching *In Situ* Measurements to Environmental Factors

We matched the *in situ* observations of GPP to contemporaneous satellite predictors according to the sampling location and date. Detailed information is provided in Table 1. In cases where ancillary data were not available, we used the corresponding monthly climatology of the missing properties. Predictors included in the training of the algorithms are expected to directly or indirectly impact or reflect primary production. For instance, temperature, nutrients and light availability have been well recognized as the main forcings driving primary production patterns at the global scale (Chavez et al., 2011). POC and Chl-*a* can be used as proxies for biomass, with the caveats that POC encompasses nonliving organic matter and that the C:Chl-*a* ratio varies as a function of taxa and growth conditions (Baker & Smith, 1982). The vertical light attenuation coefficient (K_d) can serve as a proxy for light availability as well as biomass in the water column. We also included inherent optical properties (Rrs) as they provide some information about plankton community characteristics (Li et al., 2013). Wind speed influences the delivery of nutrients to the surface through mixing. It also impacts $GPP_{17\Delta}$ by changing the mixed-layer ventilation and the residence time of O_2 at the ocean surface, thereby changing the integration timescale of the geochemical tracer. In light of our limited understanding of the mechanisms and properties regulating primary production, we let the model select the best

Table 1
Environmental properties used as predictors

Parameter	Spatial resolution	Temporal resolution	Resource	Reference
Rrs (λ)				-
SST (°C)				-
POC (mg C m^{-3})				Stramski et al. (1999)
Chl-*a* (mg m^{-3})	0.083°	8 days	Ocean color	O'Reilly et al. (1998)
PAR (Einstein m^{-2} d^{-1})				-
Euphotic zone (m)				Z. Lee et al. (2002)
K_d (m^{-1})				Z. Lee (2005)
Wind speed (m s^{-1})	2°	Daily	NCEP reanalysis	Kalnay et al. (1996)
MLD (m)	2°	3 h	Hycom	Chassignet et al. (2007)
Surface NO_3^- ($u$mol L^{-1})				
Surface PO_4^{3-} ($u$mol L^{-1})	1°	Monthly climatology	World Ocean Atlas 2013	Garcia et al. (2013)
Surface Salinity ($u$mol L^{-1})				

Rrs (λ): remote sensing reflectance above water surface at the spectral bands of 412, 442, 490, 510, 555 and 670 nm. Abbreviations: SST: sea surface temperature; POC: particulate organic carbon; Chl-a: chlorophyll-a concentration; PAR: photosynthetically available radiation; Kd: light attenuation coefficient; MLD: depth of mixed-layer.

predictors. We did not include VGPM and CbPM NPP as predictors into the machine learning algorithms in order to obtain GPP independently of other primary production models. However, similar GPP simulations were obtained when we included them in the statistical algorithms (Figure 5 and Figure S1). This is likely because NPP derived using the VGPM and CbPM models is a function of a subset of the variables we input into our statistical algorithms (see Table 1; Westberry et al., 2008). It may also suggest a similar underlying mechanism driving GPP and NPP, which is encouraging for the development of process-based GPP models based on the readily available satellite parameters.

2.3. Machine-Learning Algorithms

2.3.1. Data Processing and Selection for the Training and Validation Dataset

First, we removed data from coastal areas with bathymetry shallower than 200 m, given the difference in optical properties of Case II waters (Morel & Prieur, 1977). To limit spatial autocorrelation between observations (Tobler, 1970), the sampling data were binned into monthly 1 × 1° grids, as in Li and Cassar (2016) and Tang et al. (2019). The gridded data were natural log-transformed to satisfy the normal distribution before analysis. 392 GPP_{LD} and 922 $GPP_{17\Delta}$ gridded data points remained after these transformations. The two approaches (incubation and incubation-independent) each have their own assumptions and biases. In the absence of a benchmark method to estimate primary production (Regaudie-de-Gioux et al., 2014; Robinson et al., 2009), we derived independent algorithms for each approach and compared predictions.

2.3.2. Statistical Algorithms Based on Machine Learning and Algorithm Validation

A Pearson correlation analysis was first applied to examine the linear relationships between observed rates and individual predictors. After this preliminary analysis, the machine learning approach of Random Forest (RF) was employed to estimate global GPP. RF is an ensemble method comprised of a number of explanatory variables to predict the target output. Based on a bootstrap sampling and random selection, RF selects at each node the optimal variable to split the dataset to achieve the greatest reduction in "out-of-bag" mean square error between observation and model predictions (Liaw & Wiener, 2002). This process is repeated until some criteria are reached. RF grows a large number of decision trees and each tree mimics the structure of a hierarchical branching system. RF is not an entirely "black-box" technique and the importance of the predictors during the algorithm's construction can be used to infer some underlying mechanisms constraining GPP. More detailed information of RF can be found in Cutler et al. (2007). RF was implemented

using the function "randomForest" in the R package "randomForest" (https://cran.r-project.org/web/packages/randomForest/randomForest.pdf). The number of decision trees and minimum leaf size in our study were set at the default 500 and 3, respectively.

Independent RF analyses were conducted using GPP_{LD} and $GPP_{17\Delta}$ in the training and validation dataset. In each case, 70% of the dataset was randomly selected to train the algorithm and the remaining 30% was used for validation. To evaluate the fitness and prediction accuracy of the algorithms, we calculated the regression coefficient (R^2), and root mean standard error for pairwise real observations and model predictions of the test datasets. After the algorithm construction, the derived models were used to predict global primary production with a 2 × 2° resolution. The model output is daily GPP. The annual mean GPP presented in our study is calculated as the sum of daily rates over the annual cycle divided by the number of days (365) in a year. To test the sensitivity of our estimates to the dataset selected for training, we adopted a bootstrap approach, by repeatedly reconstructing the training dataset 500 times. For each repetition, we conducted the same analyses as described above with the reconstructed dataset to derive the global pattern of primary production, from which we calculated the mean and standard deviation for results from 500 predictions. We generally derived similar global predictions for each repetition with a standard deviation significantly smaller than the mean (Figure S2), suggesting that our statistical algorithms are insensitive to the change in the training dataset.

2.3.3. Integrating the Mixed-Layer $GPP_{17\Delta}$ Over the Euphotic Depth

The triple isotopes of dissolved oxygen approach estimates GPP in the mixed layer. GPP generally decreases with depth as a function of light availability. When the mixed-layer is deeper that the euphotic zone, the mixed-layer GPP should reflect GPP integrated over the euphotic depth. Conversely, when a mixed-layer is shallower than the euphotic depth, the mixed-layer $GPP_{17\Delta}$ underestimates the euphotic-depth GPP because it doesn't account for primary production occurring deeper in the water column where light is still available. This is particularly significant in subtropical waters where the euphotic zone often extends beyond the mixed layer (Figure S4). In regions where the mixed-layer is shallower than the euphotic depth, we scaled our mixed-layer $GPP_{17\Delta}$ to the euphotic depth using empirical relationships at different latitudes between mixed-layer GPP and euphotic-zone GPP derived from the light-dark bottle incubation (Figure S5). The model yields a global mixed-layer integrated $GPP_{17\Delta}$ of 12.9×10^{15} mol O_2 yr^{-1}, and 15.1×10^{15} mol O_2 yr^{-1} when integrated over the euphotic zone. For reference, the global pattern of mixed-layer integrated $GPP_{17\Delta}$ and GPP_{LD} are also presented in Figure s6.

2.4. Correction for Dissolved Organic Carbon Production in VGPM and CbPM Model Predictions

We compared our GPP predictions to two commonly used NPP models: CbPM and VGPM (Behrenfeld & Falkowski, 1997; Westberry et al., 2008). The VGPM model is based on chlorophyll-*a* (Chl-*a*), attributing changes in Chl-*a* to a change in biomass (Behrenfeld & Falkowski, 1997). The CbPM model is a backscattering-based estimate of phytoplankton carbon biomass from which primary production is derived (Westberry et al., 2008). As we described above, the model simulations derived from VGPM and CbPM reflect ^{14}C-based measurements, which commonly only account for POC produced NPP (NPP_{POC}; i.e., the ^{14}C data is based on filters), and therefore ignores the ^{14}C in the filtrate (i.e., $DO^{14}C$). To account for DOC production, we used the following equation suggested by Regaudie-de-Gioux et al. (2014) to derive NPP including particulate and dissolved phases (NPP_{TOC}):

$$\mathrm{LogNPP_{TOC}} = 0.67 * \mathrm{LogNPP_{POC}} + 2.25 \left(R^2 = 0.71, p < 0.001, n = 107\right) \quad (3)$$

This empirical relationship was derived from a global dataset of concurrent measurements of particulate organic carbon and total organic carbon production by ^{14}C-based incorporation approach (Regaudie-de-Gioux et al., 2014). The DOC production of 10%–60 % of NPP_{TOC} (Figure S7) is in a good agreement with the range observed in previous studies (González et al., 2008; Teira et al., 2001).

2.5. GPP Uncertainties Estimates

A Monte Carlo approach was used to propagate uncertainties in the global GPP estimates (Table 2). Randomly distributed errors were generated and 500 iterations were run to compute the standard deviation of GPP simulations.To attribute uncertainties, we altered the corresponding model settings and fixed the other model conditions as described in Sections 2.3 and 2.4. We assigned random errors of ±17% in GPP_{LD} measurements, which represents the median coefficient of variation of the light/dark incubation oxygen measurements reported in the global dataset. For $GPP_{17\Delta}$, we assigned ±30% random errors to account for the uncertainty in gas exchange velocities (Bender et al., 2011; Emerson et al., 2019). To evaluate errors associated with resolution scales, we compared global GPP simulations based on a suite of temporal (daily, monthly and monthly climatology) and spatial averaging (i.e., not binning data, and varying the grids from 0.25° to 1°). To assess the effect of different combinations of predictors on GPP estimates, we maintained the input of top-performing predictors for the model construction but randomly included or excluded other less important predictors. We restricted our analysis to the RF method with the top performing predictors Chl-*a*, POC, Rrs (412) and PAR for GPP_{LD}, and SST, Chl-*a*, PO_4^{3-} and NO_3^- for $GPP_{17\Delta}$. Spatiotemporal mismatches between the GPP observations and environmental predictors also introduce errors in our estimates. This is likely most acute when we replace missing daily properties by the corresponding monthly climatological values. We compared the difference of global GPP simulations based on the training dataset with predictors matching to 8-day averaged and monthly climatology. To assess the uncertainty associated with selecting a training dataset, we repeatedly reconstructed the training dataset 500 times and then calculated the standard deviation of derived GPP estimates. We also applied three commonly used machine learning approaches (RF, support vector regression and neural network) to construct the model with the aim of evaluating the effect of the machine learning tool on GPP estimates. Finally, we incorporated all the error sources mentioned above and calculated the propagated uncertainties in the global GPP estimates.

2.6. Caveats and Limitations

There are other sources of uncertainties in our estimates not accounted for by our analyses, including the limited number of field observations, and methodological biases associated with each type of GPP measurements. The impact of such errors on our global marine GPP estimates is difficult to quantify because they can vary regionally and temporally. For example, few GPP_{LD} observations were collected in the Southern Ocean and Pacific Ocean. A large fraction of $GPP_{17\Delta}$ were collected in the Pacific and Atlantic Oceans (Figure 1). While the factors regulating primary production differ between biomes and regions (Longhurst, 1995; Vallina et al., 2014), the machine learning approach relies on statistical relationships in the properties domain. Should the training dataset capture the range in relationships between predictors and the predictants, the machine learning model is expected to perform well. We tested the model's predictions by cross-validation using a bootstrap approach, repeatedly reconstructing the training dataset 500 times, to test the sensitivity of our estimates to the training dataset. The small standard deviation of GPP relative to the average from 500 repetitions (Figure S2 and Table 2) implies that our algorithms trained from this global dataset generally captured the factors driving the large broad-scale variability in GPP, and performed better than traditional multiple linear regression ($R^2 = 0.31$ for $GPP_{17\Delta}$ dataset and $R^2 = 0.40$ for the GPP_{LD} dataset). However, the machine learning algorithm may fail to represent the functional relation between the predictors and GPP in undersampled biomes. In these regions, our predictions should be interpreted with caution. For example, in the Southern Ocean, a region characterized by high macronutrients and low biomass in large part due to iron limitation, our model predicts relatively high GPP_{LD}. These biases are probably due to the lack of Southern Ocean GPP_{LD} observations in our training dataset, resulting in an inability of the machine learning algorithm to accurately capture the relationship between nutrients and primary production under iron limitation. Predictions should improve as more observations from a broad range of biomes are included in the training dataset. Additionally, the discrepancy in global GPP simulations between the two measurement approaches (Figures 5 and 6a) highlights the potential biases of each methodology (see the discussion in Section 4.1). In future studies, combining our purely statistical model with earth system models (e.g., to account for vertical mixing or the lack of steady-state in the geochemical tracer) and/or mechanistic models (e.g., biophysical representation of the light impact on mixed-layer integrated GPP) may help reduce uncertainties in our projections. In the discussion section, we discuss corrections for some known biases in both

Table 2
Sources of uncertainties in our global marine GPP estimates

Sources	Description of uncertainty estimates	Uncertainty (10^{15} mol O_2 yr^{-1})	
		GPP_{LD}	$GPP_{17\Delta}$
GPP measurements	Assign ±17 % error for GPP_{LD} and ±30% for $GPP_{17\Delta}$ observations	0.47	0.41
Data Subgrid	Vary the grid from 0.25°–1° and time window from daily, monthly to monthly climatology	0.2	0.14
Temporal mismatch of predictors	Match to 8-day averaged or monthly climatology predictors	0.4	0.23
Training dataset	Random reconstruction of the training dataset	0.37	0.18
Predictors input	Random selection of input predictors except for the top-performing predictors	0.16	0.30
Machine learning approach	Construct the model with different machine-learning approaches	0.7	0.5
All	Monte-Carlo uncertainty propagation	1.3	1.05

More details can be found in Section 2.5.

methods, including photorespiration for the GPP_{LD} estimates and the effects of assuming steady-state and neglecting lateral and vertical mixing on $GPP_{17\Delta}$.

3. Results

3.1. Distributions and Magnitude of GPP in the Two Datasets

We compiled 761 and 2,740 observations of GPP_{LD} and $GPP_{17\Delta}$, respectively. Most GPP_{LD} observations are from the Atlantic Ocean and the Mediterranean Sea, with limited observations in the Pacific Ocean and the Southern Ocean (Figure 1a). In contrast, the majority of $GPP_{17\Delta}$ observations were collected in the Pacific Ocean and the Southern Ocean (Figure 1d). Averaging data into monthly 1° × 1° grids returns 392 and 922 gridded data points for GPP_{LD} and $GPP_{17\Delta}$, respectively. While the seasonal distribution of GPP_{LD} is relatively homogeneous, a large fraction of $GPP_{17\Delta}$ observations were collected in January in the Southern Ocean (austral summer; Figures 1b and 1e). The GPP_{LD} observations ranged from 6.6 mmol O_2 m^{-2} d^{-1} to 1,170 mmol O_2 m^{-2} d^{-1} with a mean of 111 mmol O_2 m^{-2} d^{-1} (Figure 1c). Conversely, $GPP_{17\Delta}$ ranged between 4.1 mmol O_2 m^{-2} d^{-1} and 1,198 mmol O_2 m^{-2} d^{-1} with a mean of 154 mmol O_2 m^{-2} d^{-1} (Figure 1f).

3.2. GPP versus the Remotely Sensed Observations

The relation of GPP observations to environmental parameters and their Pearson relationships are presented in Figure 2. The GPP_{LD} observations were significantly correlated with the majority of the environmental variables (Figures 2b and 2d). GPP_{LD} were positively correlated with particulate organic carbon (POC) and Chl-*a*, light attenuation coefficient (K_d), and surface nutrients, and negatively correlated with the depth of the euphotic zone (Zeu), Rrs (443), and Rrs (488) (Figures 2a and 2b). GPP_{LD} was not correlated to mixed-layer depth, surface salinity, and wind speed (Figures 2a and 2b). $GPP_{17\Delta}$ was positively correlated with POC, Chl-*a* and K_d, and negatively correlated with Zeu, Rrs (443), and Rrs (488) (Figures 2c and 2d). Generally, the absolute values of the Pearson correlation for $GPP_{17\Delta}$ were lower than the GPP_{LD} counterparts (Figures 2c and 2d). $GPP_{17\Delta}$ were weakly or not correlated to other environmental variables (Figures 2c and 2d). Most environmental predictors are highly correlated to each other in both datasets (Figure 2).

3.3. Algorithm Validation

Overall, the slopes of the machine learning predictions versus observations for the validation dataset converged onto the identity line (Figure 3). The R^2 and root standard mean error (RSME) for GPP_{LD} were 0.55 and 0.6 mmol O_2 m^{-2} d^{-1}, respectively (Figures 3a and 3b). PAR and Chl-*a* were the two most important predictors in the construction of the GPP_{LD} algorithm by RF (Figure 4a). They explained approximately 47% of the GPP variance. The model performance marginally increased with the inclusion of other predictors (Figures 4a and 4c). The model performance for $GPP_{17\Delta}$ was slightly weaker than for GPP_{LD} ($R^2 = 0.41$), with the

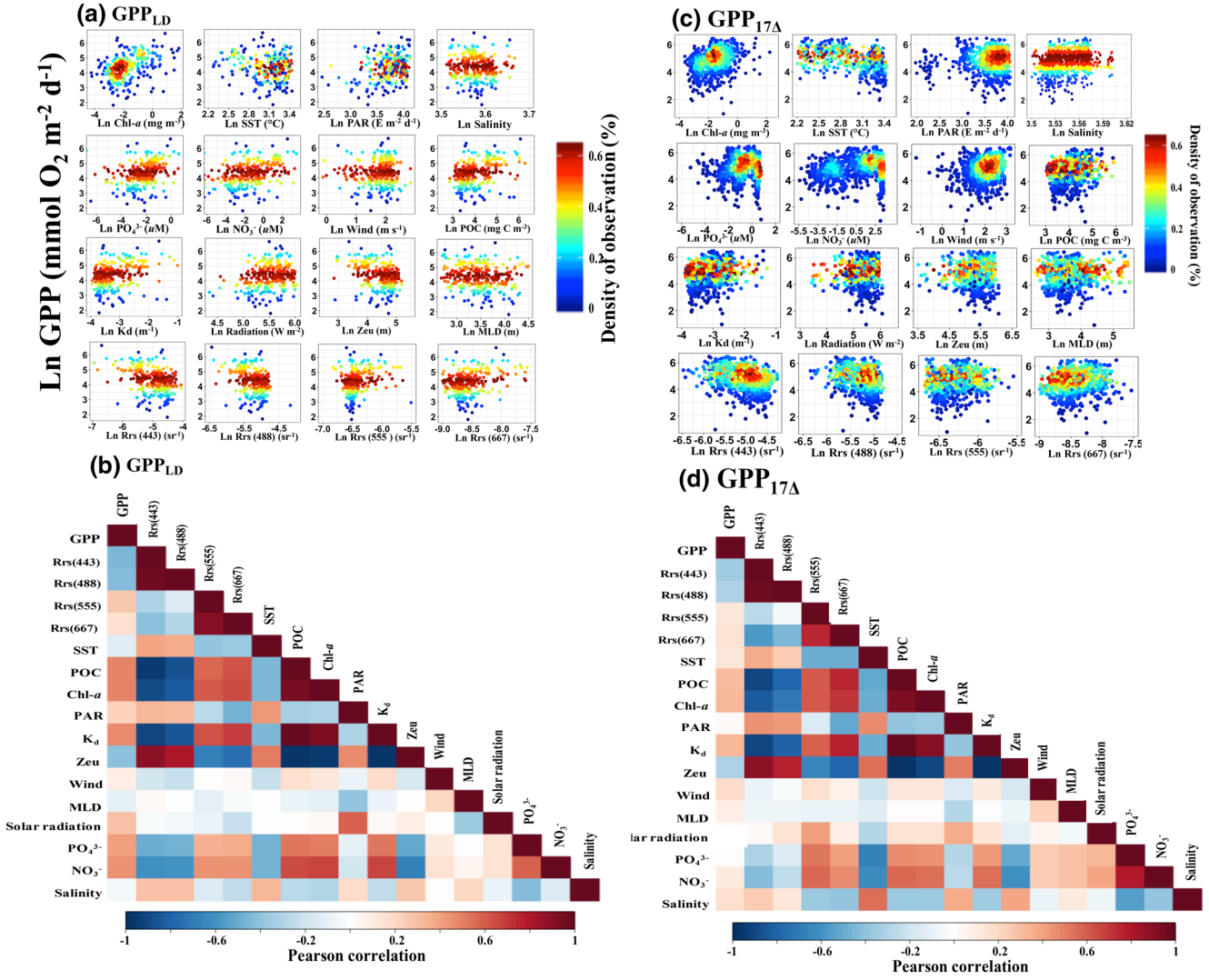

Figure 2. Scatterplots and Pearson correlation coefficients between gross primary production (GPP) and environmental properties. Point colors in panels 2a and 2c represent density of observations (Eilers & Goeman, 2004). GPP_{LD}, gross primary production derived from oxygen evolution during light-dark bottle incubations; $GPP_{17Δ}$, gross primary production derived from triple isotopes of dissolved oxygen; Rrs, inherent optical properties; SST, sea surface temperature; POC, particulate organic carbon; Chl-*a*, chlorophyll-*a*; PAR, photosynthetically available radiation; K_d, light attenuation coefficient; Zeu, depth of the euphotic zone.

R^2 and RSME being 0.44 and 0.54 mmol O_2 m^{-2} d^{-1}, respectively (Figure 4). In addition to Chl-*a*, salinity, nutrient concentrations (NO_3^- and PO_4^{3-}) and SST were selected as the top five important variables during the algorithm construction, accounting for 47% of the variance in $GPP_{17Δ}$ (Figures 4b and 4d). Generally, both GPP_{LD} and $GPP_{17Δ}$ algorithms tended to overestimate observations at the lower end (<32 mmol O_2 m^{-2} d^{-1}) and underestimate observations at the higher end (>635 mmol O_2 m^{-2} d^{-1}, Figure 3).

3.4. Global Gross Primary Production Prediction

The global patterns of GPP integrated over the euphotic zone are shown in Figure 5. Hereafter, GPP refers to GPP integrated over the euphotic zone, unless stated otherwise. The GPP_{LD} and $GPP_{17Δ}$ simulations generally agree with relatively high rates in coastal and equatorial regions, the Arabian Sea, and the Northern Hemisphere high latitudes. As expected, GPP is lower in the subtropical oceans. The annual global marine GPP_{LD} predicted by RF was 9.2 ± 1.3 × 10^{15} mol O_2 yr^{-1} (Table 3). Conversely, global $GPP_{17Δ}$ was nearly 1.6 folds higher than the GPP_{LD} estimates at 15.1 ± 1.05 × 10^{15} mol O_2 yr^{-1} (Table 3). Basin-scale rates are

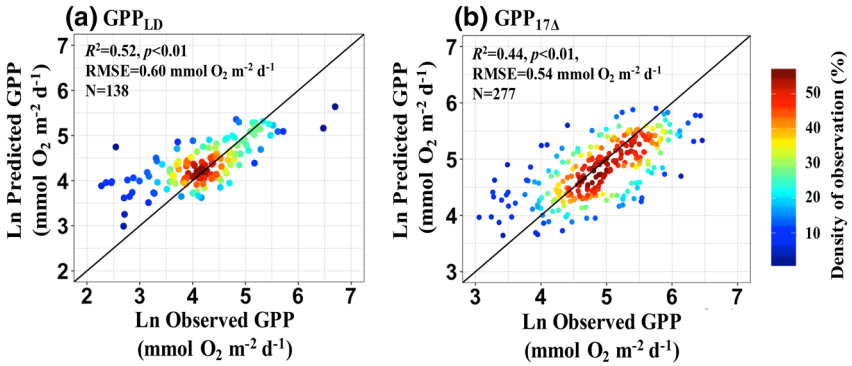

Figure 3. Evaluation of the algorithm's prediction accuracy with the validation dataset. GPP_{LD}, gross primary production derived from oxygen change during light-dark bottle incubations; $GPP_{17\Delta}$, gross primary production estimated from the triple isotopes of dissolved oxygen.

also presented in Table 3, with the Pacific and Atlantic Oceans having the highest basin-scale GPP in part because of their large surface areas.

The $GPP_{17\Delta}$ and GPP_{LD} simulations display similar meridional patterns with maxima around −40°S and in the equatorial zone (Figure 6b). As expected, the lowest GPP were simulated in the extensive subtropical ocean in the ∼5–30° meridional bands of both hemispheres (Figure 6b). The overall ratio of $GPP_{17\Delta}$ to

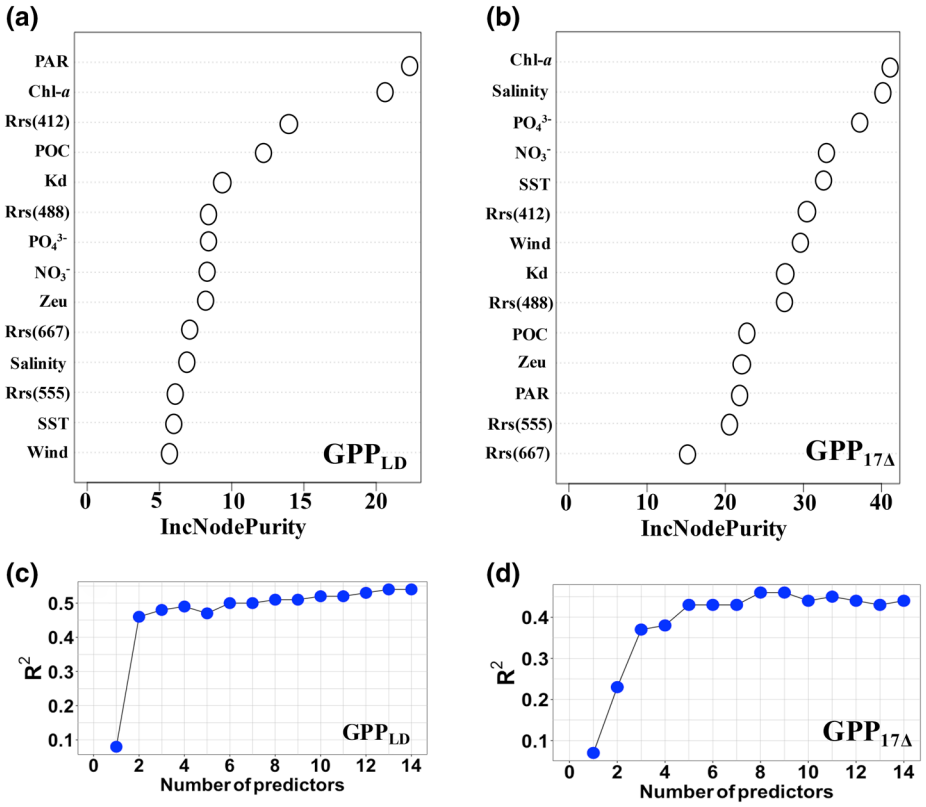

Figure 4. (a), (b) Predictor feature importance: Rank of predictor importance in the model construction by Random Forest. (c), (d) Change in model performance as a function of the number of predictors. GPP_{LD}, gross primary production derived from oxygen evolution during light-dark bottle incubations; $GPP_{17\Delta}$, gross primary production derived from triple isotopes of dissolved oxygen; Rrs, inherent optical properties; SST, sea surface temperature; POC, particulate organic carbon; Chl-*a*, chlorophyll-*a*; PAR, photosynthetically available radiation; K_d, light attenuation coefficient; Zeu, depth of the euphotic zone.

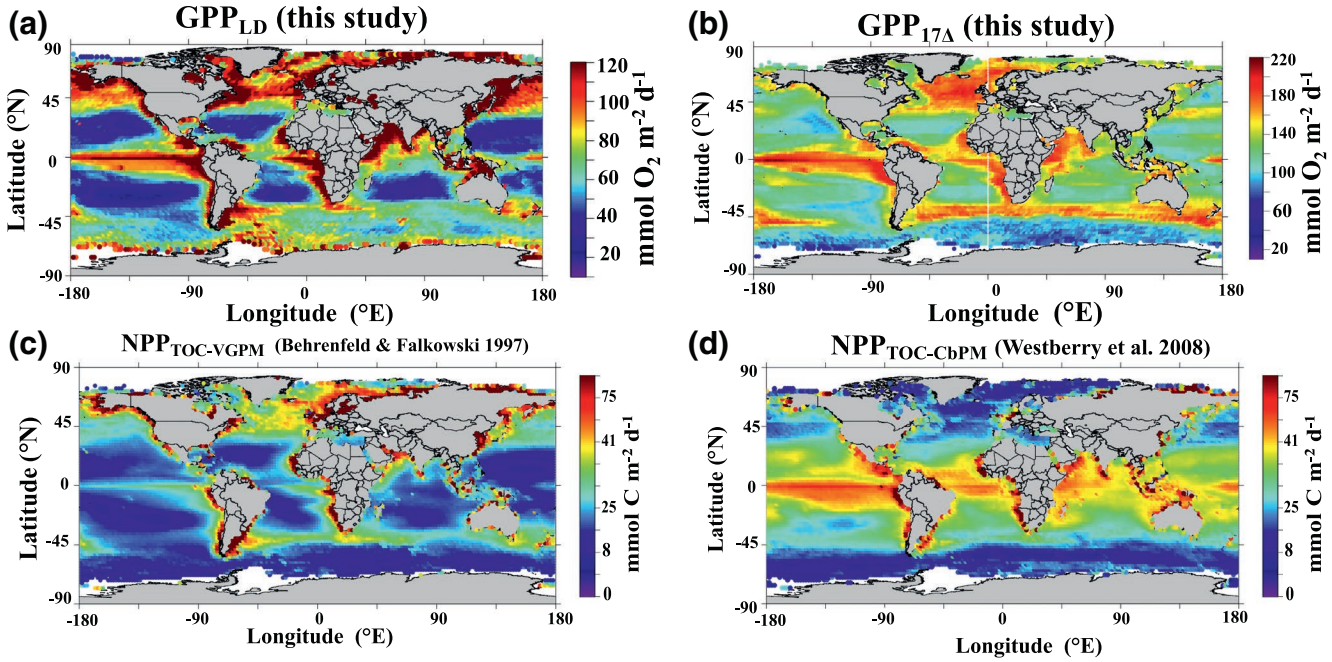

Figure 5. The global distribution of euphotic-depth GPP and NPP_{TOC}. Daily rates are calculated by summing daily rates and dividing by the number of days in a year. GPP_{LD}, gross primary production derived from oxygen change during light-dark bottle incubations; $GPP_{17Δ}$, gross primary production estimated from triple isotopes of dissolved oxygen. $NPP_{TOC-VGPM}$, net primary production including both particulate and dissolved phases corrected from VGPM model; $NPP_{TOC-CbPM}$, net primary production including both particulate and dissolved phases corrected from CbPM model.

GPP_{LD} was 1.6 (Table 3) with substantial meridional variability (Figure 6b). Differences between the two approaches peak in subtropical regions, with better agreement at lower latitudes and at high latitudes in the Northern Hemisphere. A small ratio (<1) is observed at the high latitudes of the Southern Hemisphere (Figure 6).

Table 3
Estimated gross primary production and net primary production in the world's oceans

	GPP_{LD}	$GPP_{17Δ}$	$GPP_{corrected}$	$GPP_{corrected}$	$NPP_{TOC-VGPM}$	$NPP_{TOC-CbPM}$
	10^{15} mol O_2 yr^{-1}			10^{15} mol C yr^{-1}		
Pacific	3.81 ± 0.55	6.77 ± 0.5	3.92~5.74	3.01–5.57	1.36	2.63
Atlantic	1.92 ± 0.21	3.50 ± 0.42	2.1~3.02	1.75–2.29	0.92	1.16
Indian	1.80 ± 0.27	3.41 ± 0.25	1.83~2.89	1.53–2.80	0.54	0.94
Southern Ocean	1.51 ± 0.27	1.49 ± 0.11	1.09~2.1	0.90–2.03	0.24	0.34
Arctic Ocean	0.19 ± 0.03	0.22 ± 0.02	0.18~0.19	0.15–0.18	0.12	0.05
Global	9.2 ± 1.3	15.1 ± 1.05	9.5~12.6	7.9–12.2	5.0	5.5
Reference	this study				Behrenfeld and Falkowski (1997)	Westberry et al. (2008)

Ocean basins defined as in the World Ocean Atlas 2005 (Figure S8). $GPP_{17Δ}$: gross primary production estimated from triple isotopes of dissolved oxygen. GPPcorrected: corrected gross primary production due to methodological biases (see discussion). GP was converted into the carbon unit using O_2/C elemental stoichiometry range of 1.03–1.2 (see the discussion). $NPP_{TOC-VGPM}$: net primary production including both particulate and dissolved phases corrected from VGPM model; $NPP_{TOC-CbPM}$: net primary production including both particulate and dissolved phases corrected from CbPM model.
Abbreviations: GPP, gross primary production; NPP, net primary production.

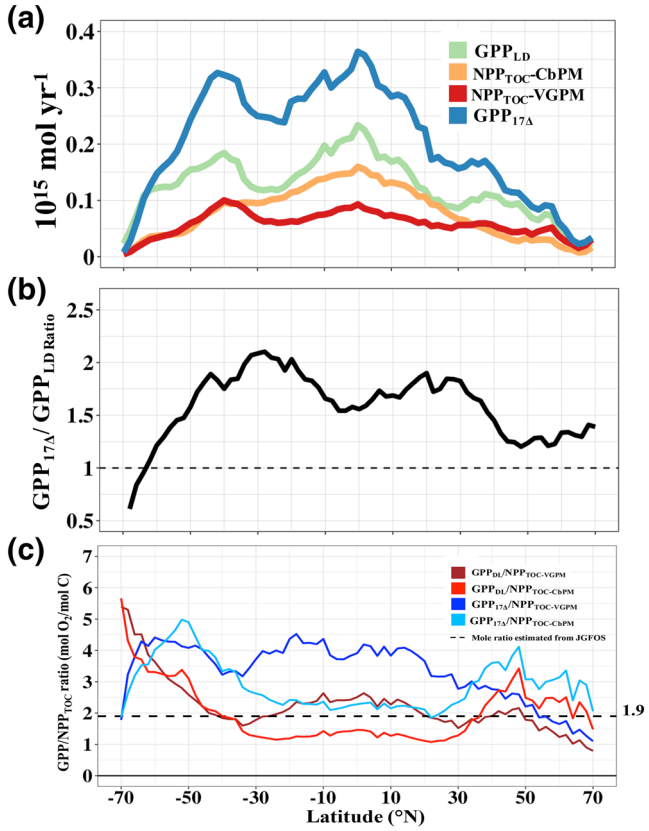

Figure 6. (a) Meridional distribution of annual marine gross primary production and net primary production and (b) meridional discrepancies between the two gross primary production simulations represented as a ratio. (c) Meridional distribution of molar ratio of GPP to NPP_{TOC} estimates. $GPP_{17\Delta}$, gross primary production estimated from triple isotopes of dissolved oxygen. $NPP_{TOC\text{-}VGPM}$, net primary production including both particulate and dissolved phases corrected from VGPM model; $NPP_{TOC\text{-}CbPM}$, net primary production including both particulate and dissolved phases adjusted from CbPM model.

4. Discussion

4.1. Discrepancies Between GPP_{LD} and $GPP_{17\Delta}$ for the Global Ocean

The global distribution of GPP derived from the machine learning upscaling of incubation and *in situ* measurements (Figures 5 and 6) are largely consistent with our understanding of the mechanisms driving primary production (Chavez et al., 2011). In winter at high latitudes, cooling and wind stress from storms destabilize the water column, bringing nutrient-rich waters to the surface thereby stimulating productivity when light is available (Taylor & Ferrari, 2011). Likewise, high GPP observed in the equatorial Pacific is fueled by the upwelling of nutrient rich waters (Barber et al., 1996). Net Ekman downwelling with stable and deep thermocline and nutricline in the subtropical ocean limits nutrient availability and primary production (Karl et al., 1996). The Southern Ocean is unique in that macronutrients are generally not fully utilized at the ocean surface due to a combination of iron and light limitation (Cassar et al., 2007; Martin et al., 1990).

At the global scale, $GPP_{17\Delta}$ is 1.6 higher than GPPLD, with the respective values of $15.1 \pm 1.05 \times 10^{15}$ mol O_2 yr^{-1} for $GPP_{17\Delta}$ and $9.2 \pm 1.3 \times 10^{15}$ mol O_2 yr^{-1} for GPP_{LD} (Table 3). This ratio is close to the 1.8 ± 0.5 value reported in the Sagami Bay by the paired comparisons of GPP determined by the same two methods (Sarma et al., 2005). More broadly, this ratio also falls within the range ($1.1 \sim 1.9$) derived from a comparison of $GPP_{17\Delta}$ to the $H_2{}^{18}O$-labeling incubation approach reported in several studies (Juranek & Quay, 2013; Luz & Barkan, 2000; Quay et al., 2010).

The $GPP_{17\Delta}$ to GPP_{LD} ratio (Figure 6b) demonstrated a pronounced meridional variability which might be explained by methodological biases in the geochemical budget approach and bottle artifacts (Elena García-Martín et al., 2011; Juranek & Quay, 2013). These methods also reflect differing time scales of GPP integration. The geochemical approach typically integrates the primary production signal over the O_2 residence time within the mixed-layer (~days to weeks), whereas the incubation-based approach reflects the rates over the incubation period. In the subtropical oligotrophic ocean, Karl et al. (2003) and Williams et al. (2004) argued that intermittent events can contribute to up to 40% of primary production. Because of their short integration time (~hours to a day), incubation-based methods may not capture episodic high GPP events potentially resulting in underestimation of primary production (compared to the geochemical tracer approach). This may in part explain the higher ratio of $GPP_{17\Delta}$ to GPP_{LD} ratio in the unproductive subtropical oligotrophic ocean (Figure 6b). The $GPP_{17\Delta}$ approach is sensitive to the influence of physical processes and the time rate of change of the triple isotope oxygen tracer. Nicholson et al. (2014) showed that vertical entrainment/mixing could result in significant biases in $GPP_{17\Delta}$ estimates, leading to underestimation of GPP at high latitudes in the Southern Hemisphere, which may explain the lower ratio of $GPP_{17\Delta}$ to GPP_{LD} we observe in these regions (Figure 6b). The model of Nicholson et al. (2014) suggests that estimates of $GPP_{17\Delta}$ are most accurate in the equatorial and low-latitude regions because advective fluxes and tracer time-rate of change are smaller. This is supported by our results which show that the ratio of $GPP_{17\Delta}$ to GPP_{LD} in these regions is closer to unity (Figure 6b).

The projected meridional variability of $GPP_{17\Delta}$ to GPP_{LD} ratio may also be attributed to biases in data distribution and methodological issues with bottle incubations. For example, the paucity of light-dark bottle incubations in the Southern Ocean and equatorial Pacific (Figure 1a) might also lead to our algorithms failing to capture the complex relationship between macronutrient and iron-limited primary production,

Table 4
Global estimates of GPP and NPP in terrestrial and marine ecosystems

Ecosystem	Variables	Value (Pg C yr^{-1})	Reference	Method
Land	GPP	119	Tramontana et al. (2016)	Statistical models scaling up observations
		112	Zhang et al. (2016)	Light use efficiency models
		123	Guanter et al. (2014)	Solar-induced fluorescence models
		130	Gent et al. (2011)	Earth System Models
		148	Kuppel et al. (2013)	Hybrid model (process-based + data-driven models)
	NPP	48	Field et al. (1998)	Satellite-based vegetation photosynthesis model
		52	Zhao and Running (2010)	Satellite-based vegetation photosynthesis model
		64	Gent et al. (2011)	Earth System Models
Ocean	GPP	103–150	This study	Statistical model scaling up observations
	NPP	60	Behrenfeld & Falkowski (1997)	VGPM model (Adjusted for DOC production)
		66	Westberry et al. (2008)	CbPM model (Adjusted for DOC production)

An elemental stoichiometry of 1.03–1.2 was used to convert marine GPP from oxygen to carbon units (see discussion).
Abbreviations: DOC, dissolved organic carbon; GPP, gross primary production; NPP, net primary production.

thereby resulting in GPP_{LD} being biased high in these regions. In addition, contamination during sampling and incubation might lead to overestimation of GPP, especially in regions where primary production is limited by trace metals such as in the Southern Ocean and equatorial Pacific (Martin et al., 1990). These two possible biases toward high GPP_{LD} could partly account for the higher GPP_{LD} projection in the Southern Ocean (Figures 6a and 6b) and lower $GPP_{17\Delta}$ to GPP_{LD} ratio in the Southern Ocean and Equatorial region (Figure 6b). The bottle incubations are also prone to errors due to confinement, which might artificially modify the growth conditions (i.e. temperature, light and nutrients) and community structure in the enclosed bottle (Huang et al., 2019). For example, Westberry et al. (2012) inferred that photosynthetic rates may be inhibited because the reduced turbulence in the bottle limits nutrient regeneration and supply to autotrophic organisms. There are also arguments that incubation-based GPP is overestimated because of the filtering out of UVB radiation by borosilicate bottles (Godoy et al., 2012). Because our understanding of these artifacts and containment effects is limited, we cannot quantitatively correct for their overall impact on estimates of GPP. Pairwise comparisons show that the ^{18}O-labeling approach generally yields higher GPP estimates than the light-dark incubation approach (Grande et al., 1989; Regaudie-de-Gioux et al., 2014). This discrepancy has been attributed in part to light-induced oxygen evolution associated with photorespiration and the Mehler reaction (Bender et al., 1999; Laws et al., 2000). The assumption of similar respiration rates under light and dark conditions in the light-dark bottle method would lead to an underestimation of GPP compared with the ^{18}O-labeling approach.

We attempt to reconcile the $GPP_{17\Delta}$ to GPP_{LD} estimates by accounting for some of the known biases in the two methods. Laws et al. (2000) estimated that a +20% correction should be applied to GPP derived from light-dark bottle estimates because they do not account for photorespiration and the Mehler reaction. Nicholson et al. (2014) suggested a −29% correction factor for $GPP_{17\Delta}$ biases associated with the effect of vertical entrainment and mixing, as discussed above. After applying these first-order corrections, the $GPP_{17\Delta}$ and GPP_{LD} converge to $9.5 \sim 12.6 \times 10^{15}$ mol O_2 yr^{-1} for the global ocean (Table 3, 4).

4.2. Comparison of GPP Simulations With Oceanic Satellite-Based NPP Models

VGPM and CbPM are two of the most-widely used algorithms to predict primary production in the global ocean (Behrenfeld & Falkowski, 1997; Westberry et al., 2008). Given that oxygen-based estimates of GPP reflect the production of particulate and dissolved organic carbon, we adjust the VGPM and CbPM NPP

estimates for DOC production for comparison to our GPP estimates. We find that our GPP simulations generally follow the pattern of NPP_{TOC} (Figures 5 and 6).

In principle, the molar ratio between primary production estimates in the units of oxygen (i.e., GPP) and carbon (i.e., NPP_{TOC}) may reflect variations in underlying metabolic pathways involved in photosynthetic gross O_2 evolution and carbon fixation. For example, the light-dependent oxygen consumption induced by the Mehler reaction and photorespiration are not associated with carbon fixation (Halsey et al., 2010; Laws et al., 2000). The photosynthetic molar ratio of O_2 evolution to C fixation is also impacted by elemental stoichiometry associated with production of proteins, polysaccharides, lipids and nucleic acids from inorganic precursors. This chemical ratio varies regionally between 1.1 and 1.4, depending among other things on the nitrogen species (ammonium or nitrate) fueling primary production (Laws, 1991). It is also affected by other factors, such as the phytoplankton's physiological optimization to the nutrient and light regime (Behrenfeld et al., 2008; Halsey et al., 2010). As discussed above, methodological biases and uncertainty in algorithm predictions may also explain differences in the primary production estimates.

The VGPM and CbPM algorithms predict a global NPP_{TOC} of 5.0×10^{15} mol C yr^{-1} and 5.5×10^{15} mol C yr^{-1}, respectively (Table 3). Combined with our corrected estimates of global marine GPP ($9.5 \sim 12.6 \times 10^{15}$ mol O_2 yr^{-1}), our study suggests a global averaged molar ratio of marine gross oxygen to net carbon production of 1.7–2.5. This molar ratio is lower than observations based on O_2 and C incubations from culture studies (3.3 mol O_2/C; Halsey & Jones, 2015; Halsey et al., 2010) and Joint Global Flux Study (2.7 mol O_2/C; Juranek & Quay, 2013). It is worth noting that the ^{14}C-based incubation in these studies only account for particulate phase organic production. A first-order correction of these estimates for DOC production (assuming 20%–30% of TOC production is DOC production) brings these ratios in the same range as our estimates ($2.3 \sim 2.6$ and $1.89 \sim 2.16$, respectively). Meridional variations in the molar ratio of primary production estimates in the unit of oxygen and carbon are highly uncertain and dependent on the algorithm used (Figure 6c). As is the case for the GPP algorithms GPP, satellite estimates of NPP carry uncertainties, as shown by comparisons with field measurements of ^{14}C-based primary production (Friedrichs et al., 2009; Palevsky et al., 2016; Regaudie-de-Gioux et al., 2019; Saba et al., 2010). Using VGPM versus CbPM leads to large differences in predicted GPP/NPP (GPP/NPP, mol O_2/mol C), especially in the subtropical and tropical area (Figure 6c).

Applying the global average scaling factor (corrected to 1.8–2.16, see the above discussion above; Juranek & Quay, 2013) as a basis to identify the latitudinal variability in the oxygen to carbon ratio, we generally observe a consistently higher deviation at the high latitude of the Southern Hemisphere (mainly in the Southern Ocean), although there is substantial noise (Figure 6c). It is unclear whether this reflects systematic methodological biases in the Southern Ocean (i.e., the effect of mixing/vertical diffusion in triple isotopic oxygen signal) or provides some insight into phytoplankton physiology (e.g., iron deficiency) and nutrient distribution (e.g., nitrogen species). Also, a comparison of the latitudinal trends in NPP_{TOC} and GPP is compromised by the uncertainty associated with the empirical conversion of POC-based NPP to TOC-based NPP. Earlier studies show that the ratio of DOC:POC production varies regionally by a factor of three and is correlated with the nutrient status and microbial community structure (Roshan and DeVries, 2017). Further work is needed to test the modeled meridional variability in the molar O_2/C ratio.

We can also, at first order, attribute the difference between GPP and NPP to autotrophic carbon loss (Dring et al., 1982; Marra, 2009). Conversion of GPP to carbon units is not trivial. Primary production is fueled by "new" (mainly in the form of nitrate) and "regenerated" nitrogen (mainly in the form of ammonium). The O_2/C elemental stoichiometries for (new) nitrate and (regenerated) ammonium-fueled primary production are 1.4 ± 0.1 and 1.1 ± 0.1, respectively (Dugdale & Goering, 1967; Laws, 1991). The f-ratio, defined as the ratio of new production to total primary production is around 0.1–0.25 globally (Dunne et al., 2007; Henson et al., 2011; Siegel et al., 2014). Based on this information and neglecting the contribution of N_2 fixation (Tang et al., 2019), the uncertainty for the global averaged C:O ratio for GPP likely ranges between 1.03 ($=1 \times 0.9 + 1.3 \times 0.1$) and 1.2 ($0.25 \times 1.1 + 1.5 \times 0.75$). Applying this range of elemental stoichiometries to convert oxygen to carbon-based primary production (our corrected GPP simulations), we find that our global oceanic GPP ranges from 103 to 150 Pg C yr^{-1} (Table 4). Our estimates of marine GPP only account for primary production generated by planktonic communities within the photic zone. However, this should represent the largest fraction of marine GPP, as global NPP in other marine biomes are comparatively small with benthic microalgae at 0.32 Pg C yr^{-1} (Gattuso et al., 2006), marine marcrophytes at 1 Pg C yr^{-1}

(Smith, 1981) and chemoautotrophs at 0.7 Pg C yr^{-1} (Middelburg, 2011). The contribution of these other biomes to GPP is therefore likely within the uncertainty of our global marine GPP estimates. Our estimates of global marine GPP (103–150 Pg C yr^{-1}) is 1.5–2.2 fold greater than oceanic NPP and comparable to terrestrial GPP rates (112–148 Pg C yr^{-1}, Table 4).

5. Conclusion

Our study represents a first attempt to assess the global distribution of O_2-based oceanic GPP thereby providing novel insight into marine primary production and its role in carbon cycling. Global GPP derived from the two datasets displayed similar patterns and are in general agreement with our current understanding of the geographical distribution of primary production. The observed discrepancy of GPP between the incubation-based and geochemical approaches at certain latitudes deserves further investigation. In particular, current biases, such as the effect of vertical mixing on the triple isotope signature of oxygen, could be corrected for in a spatiotemporally explicit manner in future studies using model predictions. After accounting for some of these biases, global marine GPP estimates of 103–150 Pg C yr^{-1} are comparable to GPP on land.

Data Availability Statement

The authors are grateful to collaborators for contributing their data to this project. This study benefited from discussions with Dr. E. Laws at Louisiana State University and Dr. Y. Xie at the National Oceanic and Atmospheric Administration. The compiled datasets for gross primary production are presented in the supporting information (Table S1). Satellite data, wind speed, nutrients concentrations, net primary production and monthly MLD climatology were downloaded from NASA Ocean Color (http://oceancolor.gsfc.nasa.gov/cms/), NCEP/NCAR reanalysis (https://www.esrl.noaa.gov/psd/data/gridded/data.ncep.reanalysis.html), World Ocean Atlas (https://www.nodc.noaa.gov/OC5/woa13/), https://www.science.oregonstate.edu/ocean.productivity/, and www.ifremer.fr/cerweb/deboyer/mld/home.php, respectively. The monthly GPP products developed in our study are available via ZENODO (https://zenodo.org/record/4455883#.YBB_DJNKhhE) or Cassar's lab website (https://sites.nicholas.duke.edu/cassar/).

Acknowledgments
N. Cassar was supported by the "Laboratoire d'Excellence" LabexMER (ANR-10-LABX-19) and co-funded by a grant from the French government under the program "Investissements d'Avenir." Y. Huang and B. Huang were supported by grants from the National Key and Development Program of China (No.2016YFA0601201) and China NSF (No.41890803, U1805241). Y. Huang was also partly supported by Chinese State Scholarship Fund to study at Duke University as a joint Ph. D student (No. 201806310052). D. Nicholson was supported by NASA OBB NNX16AR48 G and NASA 80NSSC17K0663 and an Early Career Award from the Woods Hole Oceanographic Institution.

References

Anav, A., Friedlingstein, P., Beer, C., Ciais, P., Harper, A., Jones, C., et al. (2015). Spatiotemporal patterns of terrestrial gross primary production: A review. *Reviews of Geophysics*, *53*(3), 785–818. https://doi.org/10.1002/2015rg000483

Ash, J. L., Hu, H., & Yeung, L. Y. (2020). What fractionates oxygen isotopes during respiration? Insights from multiple isotopologue measurements and theory. *ACS Earth and Space Chemistry*, *4*(1), 50–66. https://doi.org/10.1021/acsearthspacechem.9b00230

Baker, K. S., & Smith, R. C. (1982). Bio-optical classification and model of natural waters. 21. *Limnology & Oceanography*, *27*(3), 500–509. https://doi.org/10.4319/lo.1982.27.3.0500

Barber, R. T., Sanderson, M. P., Lindley, S. T., Chai, F., Newton, J., Trees, C. C., et al. (1996). Primary productivity and its regulation in the equatorial Pacific during and following the 1991–1992 El Niño. *Deep Sea Research Part II: Topical Studies in Oceanography*, *43*(4–6), 933–969. https://doi.org/10.1016/0967-0645(96)00035-5

Beer, C., Reichstein, M., Tomelleri, E., Ciais, P., Jung, M., Carvalhais, N., et al. (2010). Terrestrial gross carbon dioxide uptake: Global distribution and covariation with climate. *Science*, *329*(5993), 834–838. https://doi.org/10.1126/science.1184984

Behrenfeld, M. J., & Falkowski, P. G. (1997). Photosynthetic rates derived from satellite-based chlorophyll concentration. *Limnology & Oceanography*, *42*(1), 1–20. https://doi.org/10.4319/lo.1997.42.1.0001

Behrenfeld, M. J., Halsey, K. H., & Milligan, A. J. (2008). Evolved physiological responses of phytoplankton to their integrated growth environment. *Philosophical Transactions of the Royal Society B: Biological Sciences*, *363*(1504), 2687–2703. https://doi.org/10.1098/rstb.2008.0019

Bender, M., Grande, K., Johnson, K., Marra, J., Williams, P. J. L., Sieburth, J., et al. (1987). A comparison of four methods for determining planktonic community production. *Limnology & Oceanography*, *32*(5), 1085–1098. https://doi.org/10.4319/lo.1987.32.5.1085

Bender, M. L., Kinter, S., Cassar, N., & Wanninkhof, R. (2011). Evaluating gas transfer velocity parameterizations using upper ocean radon distributions. *Journal of Geophysical Research-Ocean*, *116*(C2). https://doi.org/10.1029/2009JC005805

Bender, M., Orchardo, J., Dickson, M.-L., Barber, R., & Lindley, S. (1999). In vitro O_2 fluxes compared with ^{14}C production and other rate terms during the JGOFS Equatorial Pacific experiment. *Deep Sea Research Part I Oceanographic Research Papers*, *46*(4), 637–654. https://doi.org/10.1016/S0967-0637(98)00080-6

Carlson, C. A., & Hansell, D. A. (2015). *DOM sources, sinks, reactivity, and budgets. Biogeochemistry of marine dissolved organic matter* (pp. 65–126) Elsevier. https://doi.org/10.1016/B978-0-12-405940-5.00003-0

Carvalho, M. C., Schulz, K. G., & Eyre, B. D. (2017). Respiration of new and old carbon in the surface ocean: Implications for estimates of global oceanic gross primary productivity. *Global Biogeochemical Cycles*, *31*(6), 975–984. https://doi.org/10.1002/2016GB005583

Cassar, N., Bender, M. L., Barnett, B. A., Fan, S., Moxim, W. J., Levy, H., 2nd, & Tilbrook, B. (2007). The Southern Ocean biological response to aeolian iron deposition. *Science*, *317*(5841), 1067–1070. https://doi.org/10.1126/science.1144602

Chassignet, E. P., Hurlburt, H. E., Smedstad, O. M., Halliwell, G. R., Hogan, P. J., Wallcraft, A. J., et al. (2007). The HYCOM (HYbrid Coordinate Ocean Model) data assimilative system. *Journal of Marine Systems*, *65*(1), 60–83. https://doi.org/10.1016/j.jmarsys.2005.09.016

Chavez, F. P., Messie, M., & Pennington, J. T. (2011). Marine primary production in relation to climate variability and change. *Annual Review Marine Science*, *3*(1), 227–260. https://doi.org/10.1146/annurev.marine.010908.163917

Cutler, D. R., Edwards, T. C., Jr., Beard, K. H., Cutler, A., Hess, K. T., Gibson, J., & Lawler, J. J. (2007). Random forests for classification in ecology. *Ecology*, *88*(11), 2783–2792. https://doi.org/10.1890/07-0539.1

Dring, M. J., Jewson, D. H., & Fogg, G. E. (1982). What does ^{14}C uptake by phytoplankton really measure? A theoretical modeling approach. *Proceedings of the Royal Society of London. Series B. Biological Sciences*, *214*(1196), 351–368. https://doi.org/10.1098/rspb.1982.0016

Dugdale, R. C., & Goering, J. J. (1967). Uptake of new and regenerated forms of nitrogen in primary productivity. *Limnology & Oceanography*, *12*(2), 196–&. https://doi.org/10.4319/lo.1967.12.2.0196

Dunne, J. P., Sarmiento, J. L., & Gnanadesikan, A. (2007). A synthesis of global particle export from the surface ocean and cycling through the ocean interior and on the seafloor. *Global Biogeochemical Cycles*, *21*(4), GB4006. https://doi.org/10.1029/2006gb002907

Eilers, P. H. C., & Goeman, J. J. (2004). Enhancing scatterplots with smoothed densities. *Bioinformatics*, *20*(5), 623–628. https://doi.org/10.1093/bioinformatics/btg454

Elena García-Martín, E., Serret, P., & Pérez-Lorenzo, M. (2011). Testing potential bias in marine plankton respiration rates by dark bottle incubations in the NW Iberian shelf: Incubation time and bottle volume. *Continental Shelf Research*, *31*(5), 496–506. https://doi.org/10.1016/j.csr.2010.07.006

Emerson, S., Yang, B., White, M., & Cronin, M. (2019). Air-sea gas transfer: Determining bubble fuxes with iIn situ N_2 observations. *Journal of Geophysical Research: Oceans*, *124*(4), 2716–2727. https://doi.org/10.1029/2018jc014786

Field, C. B., Behrenfeld, M. J., Randerson, J. T., & Falkowski, P. (1998). Primary production of the biosphere: Integrating terrestrial and oceanic components. *Science*, *281*(5374), 237–240. https://doi.org/10.1126/science.281.5374.237

Friedrichs, M. A. M., Carr, M.-E., Barber, R. T., Scardi, M., Antoine, D., Armstrong, R. A., et al. (2009). Assessing the uncertainties of model estimates of primary productivity in the tropical Pacific Ocean. *Journal of Marine Systems*, *76*(1–2), 113–133. https://doi.org/10.1016/j.jmarsys.2008.05.010

Gaarder, T., & Gran, H. H. (1927). Investigations of the production of plankton in the Oslo Fjord. *Rapports et Proces-verbaux des reunions. Conseil International pour 1'Exploration de la Mer*, *42*(42), 1–48.

Garcia, H. E., & Gordon, L. I. (1992). Oxygen solubility in seawater-better fitting equations. *Limnology & Oceanography*, *37*(6), 1307–1312. https://doi.org/10.4319/lo.1992.37.6.1307

Garcia, H. E., Locarnini, R. A., Boyer, T. P., Antonov, J. I., Baranova, O. K., Zweng, M. M., et al. (2013). *World ocean atlas 2013*. In: Dissolved Inorganic Nutrients (Phosphate, Nitrate, Silicate), Vol. 4.

Gattuso, J.-P., Gentili, B., Duarte, C. M., Kleypas, J. A., Middelburg, J. J., & Antoine, D. (2006). Light availability in the coastal ocean: Impact on the distribution of benthic photosynthetic organisms and their contribution to primary production. *Biogeosciences*, *3*(4), 489–513. https://doi.org/10.5194/bg-3-489-2006,2006

Gent, P. R., Danabasoglu, G., Donner, L. J., Holland, M. M., Hunke, E. C., Jayne, S. R., et al. (2011). The community climate system model version 4. *Journal of Climate*, *24*(19), 4973–4991. https://doi.org/10.1175/2011jcli4083.1

Godoy, N., Canepa, A., Lasternas, S., Mayol, E., Ruíz-Halpern, S., Agustí, S., et al. (2012). Experimental assessment of the effect of UVB radiation on plankton community metabolism along the Southeastern Pacific off Chile. *Biogeosciences*, *9*(4), 1267–1276. https://doi.org/10.5194/bg-9-1267-2012

González, N., Gattuso, J. P., & Middelburg, J. J. (2008). Oxygen production and carbon fixation in oligotrophic coastal bays and the relationship with gross and net primary production. *Aquatic Microbial Ecology*, *52*(2), 119–130. https://doi.org/10.3354/ame01208

Grande, K. D., Williams, P. J. L., Marra, J., Purdie, D. A., Heinemann, K., Eppley, R. W., & Bender, M. L. (1989). Primary production in the north Pacific gyre: A comparison of rates determined by the ^{14}C, O_2 concentration and ^{18}O methods. *Deep-Sea Research A Oceanographic Research Papers*, *36*(11), 1621–1634. https://doi.org/10.1016/0198-0149(89)90063-0

Guanter, L., Zhang, Y., Jung, M., Joiner, J., Voigt, M., Berry, J. A., et al. (2014). Global and time-resolved monitoring of crop photosynthesis with chlorophyll fluorescence. *Proceedings of the National Academy of Sciences*, *111*(14), E1327–E1333. https://doi.org/10.1073/pnas.1320008111

Halsey, K. H., & Jones, B. M. (2015). Phytoplankton strategies for photosynthetic energy allocation. *Annual Review Marine Science*, *7*, 265–297. https://doi.org/10.1146/annurev-marine-010814-015813

Halsey, K. H., Milligan, A. J., & Behrenfeld, M. J. (2010). Physiological optimization underlies growth rate-independent chlorophyll-specific gross and net primary production. *Photosynthesis Research*, *103*(2), 125–137. https://doi.org/10.1007/s11120-009-9526-z

Hamme, R. C., Cassar, N., Lance, V. P., Vaillancourt, R. D., Bender, M. L., Strutton, P. G., et al. (2012). Dissolved O_2/Ar and other methods reveal rapid changes in productivity during a Lagrangian experiment in the Southern Ocean. *Journal of Geophysical Research*, *117*(C4). https://doi.org/10.1029/2011JC007046

Helman, Y., Barkan, E., Eisenstadt, D., Luz, B., & Kaplan, A. (2005). Fractionation of the three stable oxygen isotopes by oxygen-producing and oxygen-consuming reactions in photosynthetic organisms. *Plant Physiology*, *138*(4), 2292–2298. https://doi.org/10.1104/pp.105.063768

Henson, S. A., Sanders, R., Madsen, E., Morris, P. J., Le Moigne, F., & Quartly, G. D. (2011). A reduced estimate of the strength of the ocean's biological carbon pump. *Geophysical Research Letters*, *38*(4). https://doi.org/10.1029/2011gl046735

Hosoda, S., Ohira, T., Sato, K., & Suga, T. (2010). Improved description of global mixed- layer depth using Argo profiling floats. *Journal of Oceanography*, *66*(6), 773–787. https://doi.org/10.1007/s10872-010-0063-3

Huang, Y., Chen, B., Huang, B., Zhou, H., & Yuan, Y. (2019). Potential overestimation of community respiration in the western Pacific boundary ocean: What causes the putative net heterotrophy in oligotrophic systems? *Limnology & Oceanography*, *64*(5), 2202–2219. https://doi.org/10.1002/lno.11179

Juranek, L. W., & Quay, P. D. (2005). In vitro and in situ gross primary and net community production in the North Pacific Subtropical Gyre using labeled and natural abundance isotopes of dissolved O_2. *Global Biogeochemical Cycles*, *19*(3). https://doi.org/10.1029/2004gb002384

Juranek, L. W., & Quay, P. D. (2013). Using triple isotopes of dissolved oxygen to evaluate global marine productivity. *Annual Review Marine Science*, *5*, 503–524. https://doi.org/10.1146/annurev-marine-121211-172430

Kaiser, J. (2011). Technical note: Consistent calculation of aquatic gross production from oxygen triple isotope measurements. *Biogeosciences*, *8*(7), 1793–1811. https://doi.org/10.5194/bg-8-1793-2011

Kalnay, E., Kanamitsu, M., Kistler, R., Collins, W., Deaven, D., Gandin, L., et al. (1996). The NCEP/NCAR 40-year reanalysis project. *Bulletin of the American Meteorological Society*, *77*(3), 437–471. https://doi.org/10.1175/1520-0477(1996)077<0437:TNYRP>2.0.CO;2

Karl, D. M., Christian, J. R., Dore, J. E., Hebel, D. V., Letelier, R. M., Tupas, L. M., & Winn, C. D. (1996). Seasonal and interannual variability in primary production and particle flux at Station ALOHA. *Deep Sea Research Part II: Topical Studies in Oceanography*, *43*(2–3), 539–568. https://doi.org/10.1016/0967-0645(96)00002-1

Karl, D. M., Laws, E. A., Morris, P., Williams, P. J. l., & Emerson, S. (2003). Metabolic balance of the open sea. *Nature*, *426*(6962), 32. https://doi.org/10.1038/426032a

Kolber, Z. S., Prasil, O., & Falkowski, P. G. (1998). Measurements of variable chlorophyll fluorescence using fast repetition rate techniques: Defining methodology and experimental protocols. *Biochimica et Biophysica Acta (BBA) – Bioenergetics*, *1367*(1–3), 88–106. https://doi.org/10.1016/S0005-2728(98)00135-2

Kuppel, S., Chevallier, F., & Peylin, P. (2013). Quantifying the model structural error in carbon cycle data assimilation systems. *Geoscience Model Development*, *6*(1), 45–55. https://doi.org/10.5194/gmd-6-45-2013

Lämmerzahl, P., Röckmann, T., Brenninkmeijer, C. A. M., Krankowsky, D., & Mauersberger, K. (2002). Oxygen isotope composition of stratospheric carbon dioxide. *Geophysical Research Letters*, *29*(12), 23–24. https://doi.org/10.1029/2001GL014343

Laws, E. A. (1991). Photosynthetic quotients, new production and net community production in the open ocean. *Deep-Sea Research A-Oceanographic Research Papers*, *38*(1), 143–167. https://doi.org/10.1016/0198-0149(91)90059-O

Laws, E. A., Landry, M. R., Barber, R. T., Campbell, L., Dickson, M.-L., & Marra, J. (2000). Carbon cycling in primary production bottle incubations: Inferences from grazing experiments and photosynthetic studies using and in the Arabian Sea. *Deep Sea Research Part II: Topical Studies in Oceanography*, *47*(7–8), 1339–1352. https://doi.org/10.1016/s0967-0645(99)00146-0

Lee, Z. (2005). A model for the diffuse attenuation coefficient of downwelling irradiance. *Journal of Geophysical Research*, *110*(C2). https://doi.org/10.1029/2004jc002275

Lee, Z., Carder, K. L., & Arnone, R. A. (2002). Deriving inherent optical properties from water color:A multiband quasi-analytical algorithm for optically deep waters. *Applied Optics*, *41*(27), 5755–5772. https://doi.org/10.1364/ao.41.005755

Lee, T. R., Wood, W. T., & Phrampus, B. J. (2019). A machine learning (kNN) approach to predicting global seafloor total organic carbon. *Global Biogeochemical Cycles*, *33*(1), 37–46. https://doi.org/10.1029/2018gb005992

Letscher, R. T., & Moore, J. K. (2017). Modest net autotrophy in the oligotrophic ocean. *Global Biogeochemical Cycles*, *31*, 699–708. https://doi.org/10.1002/2016GB005503

Liaw, A., & Wiener, M. (2002). Classification and regression by randomForest. *R News*, *2*(3), 18–22. https://doi.org/10.1002/2016GB005503

Li, Z., & Cassar, N. (2016). Satellite estimates of net community production based on O_2/Ar observations and comparison to other estimates. *Global Biogeochemical Cycles*, *30*(5), 735–752. https://doi.org/10.1002/2015GB005314

Li, Z., Li, L., Song, K., & Cassar, N., (2013). Estimation of phytoplankton size fractions based on spectral features of remote sensing ocean color data. *Journal of Geophysical Research 118* (3), 1445–1458. https://doi.org/10.1002/jgrc.20137

Longhurst, A. (1995). Seasonal cycles of pelagic production and consumption. *Progress in Oceanography*, *36*(2), 77–167. https://doi.org/10.1016/0079-6611(95)00015-1

Luz, B., & Barkan, E. (2000). Assessment of oceanic productivity with the triple-isotope composition of dissolved oxygen. *Science*, *288*(5473), 2028–2031. https://doi.org/10.1126/science.288.5473.2028

Luz, B., & Barkan, E. (2005). The isotopic ratios $^{17}O/^{16}O$ and $^{18}O/^{16}O$ in molecular oxygen and their significance in biogeochemistry. *Geochimica et Cosmochimica Acta*, *69*(5), 1099–1110. https://doi.org/10.1016/j.gca.2004.09.001

Marra, J. (2009). Net and gross productivity: Weighing in with 14C. *Aquatic Microbial Ecology*, *56*(2–3), 123–131. https://doi.org/10.3354/ame01306

Martin, J. H., Fitzwater, S. E., & Gordon, R. M. (1990). Iron deficiency limits phytoplankton growth in Antarctic waters. *Global Biogeochemical Cycles*, *4*(1), 5–12. https://doi.org/10.1029/GB004i001p00005

Mazzocchi, M. G., Siokou, I., Tirelli, V., Bandelj, V., Fernandez de Puelles, M. L., Ak Örek, Y., et al. (2014). Regional and seasonal characteristics of epipelagic mesozooplankton in the Mediterranean Sea based on an artificial neural network analysis. *Journal of Marine Systems*, *135*, 64–80. https://doi.org/10.1016/j.jmarsys.2013.04.009

Middelburg, J. J. (2011). Chemoautotrophy in the ocean. *Geophysical Research Letters*, *38*(24). https://doi.org/10.1029/2011GL049725

Moore, J. K., Lindsay, K., Doney, S. C., Long, M. C., & Misumi, K. (2013). Marine ecosystem dynamics and biogeochemical cycling in the community earth system model [CESM1(BGC)]: Comparison of the 1990s with the 2090s under the RCP4.5 and RCP8.5 scenarios. *Journal of Climate*, *26*(23), 9291–9312. https://doi.org/10.1175/Jcli-D-12-00566.1

Morel, A., & Prieur, L. (1977). Analysis of variations in ocean color1. *Limnology & Oceanography*, *22*(4), 709–722. https://doi.org/10.4319/lo.1977.22.4.0709

Myklestad, S. M. (2000). Dissolved organic carbon from phytoplankton. *Handbook of Environmental Chemistry*, 111–148. https://doi.org/10.1007/10683826_5

Nicholson, D., Emerson, S., & Eriksen, C. C. (2008). Net community production in the deep euphotic zone of the subtropical North Pacific gyre from glider surveys. *Limnology & Oceanography*, *53*(5), 2226–2236. https://doi.org/10.4319/lo.2008.53.5_part_2.2226

Nicholson, D., Stanley, R. H. R., & Doney, S. C. (2014). The triple oxygen isotope tracer of primary productivity in a dynamic ocean model. *Global Biogeochemical Cycles*, *28*(5), 538–552. https://doi.org/10.1002/2013gb004704

O'Reilly, J. E., Maritorena, S., Mitchell, B. G., Siegel, D. A., Carder, K. L., Garver, S. A., et al. (1998). Ocean color chlorophyll algorithms for SeaWiFS. *Journal of Geophysical Research*, *103*(C11), 24937–24953. https://doi.org/10.1029/98JC02160

Palevsky, H. I., Quay, P. D., & Nicholson, D. P. (2016). Discrepant estimates of primary and export production from satellite algorithms, a biogeochemical model, and geochemical tracer measurements in the North Pacific Ocean. *Geophysical Research Letters*, *43*(16), 8645–8653. https://doi.org/10.1002/2016GL070226

Peterson, B. J. (1980). Aquatic primary productivity and the^{14}C-CO_2 method: A history of the productivity problem. *Annual Review of Ecology and Systematics*, *11*(11), 359–385. https://doi.org/10.1146/annurev.es.11.110180.002043

Prokopenko, M. G., Pauluis, O. M., Granger, J., & Yeung, L. Y. (2011). Exact evaluation of gross photosynthetic production from the oxygen triple-isotope composition of O_2: Implications for the net-to-gross primary production ratios. *Geophysical Research Letters*, *38*(14). https://doi.org/10.1029/2011gl047652

Quay, P. D., Peacock, C., Björkman, K., & Karl, D. M. (2010). Measuring primary production rates in the ocean: Enigmatic results between incubation and non- incubation methods at Station ALOHA. *Global Biogeochemical Cycles*, *24*(3). https://doi.org/10.1029/2009GB003665

Regaudie-de-Gioux, A., Huete-Ortega, M., Sobrino, C., López-Sandoval, D. C., González, N., Fernández-Carrera, A., et al. (2019). Multi-model remote sensing assessment of primary production in the subtropical gyres. *Journal of Marine Systems*, *196*, 97–106. https://doi.org/10.1016/j.jmarsys.2019.03.007

Regaudie-de-Gioux, A., Lasternas, S. b., AgustÃ, S., & Duarte, C. M. (2014). Comparing marine primary production estimates through different methods and development of conversion equations. *Frontiers in Marine Science*, *1*(19). https://doi.org/10.3389/fmars.2014.00019

Reuer, M. K., Barnett, B. A., Bender, M. L., Falkowski, P. G., & Hendricks, M. B. (2007). New estimates of Southern Ocean biological production rates from O2/Ar ratios and the triple isotope composition of O2. *Deep Sea Research Part I: Oceanographic Research Papers*, *54*(6), 951–974. https://doi.org/10.1016/j.dsr.2007.02.007

Robinson, C., Tilstone, G. H., Rees, A. P., Smyth, T. J., Fishwick, J. R., Tarran, G. A., et al. (2009). Comparison of in vitro and in situ plankton production determinations. *Aquatic Microbial Ecology*, *54*(1), 13–34. https://doi.org/10.3354/ame01250

Roshan, S., & DeVries, T. (2017). Efficient dissolved organic carbon production and export in the oligotrophic ocean. *Nature Communications*, *8*, 2036. https://doi.org/10.1038/s41467-017-02227-3

Saba, V. S., Friedrichs, M. A. M., Carr, M. E., Antoine, D., Armstrong, R. A., Asanuma, I., et al. (2010). Challenges of modeling depth-integrated marine primary productivity over multiple decades: A case study at BATS and HOT. *Global Biogeochemical Cycles*, *24*(3). https://doi.org/10.1029/2009gb003655

Sarma, V. V. S. S., Abe, O., Hashimoto, S., Hinuma, A., & Saino, T. (2005). Seasonal variations in triple oxygen isotopes and gross oxygen production in the Sagami Bay, central Japan. *Limnology & Oceanography*, *50*(2), 544–552. https://doi.org/10.4319/lo.2005.50.2.0544

Serret, P., Fernandez, E., Sostres, J. A., & Anadon, R. (1999). Seasonal compensation of microbial production and respiration in a temperate sea. *Marine Ecology Progress Series*, *187*(187), 43–57. https://doi.org/10.3354/meps187043

Serret, P., Robinson, C., Aranguren-Gassis, M., Garcia-Martin, E. E., Gist, N., Kitidis, V., et al. (2015). Both respiration and photosynthesis determine the scaling of plankton metabolism in the oligotrophic ocean. *Nature Communications*, *6*(1), 6961. https://doi.org/10.1038/ncomms7961

Siegel, D. A., Buesseler, K. O., Doney, S. C., Sailley, S. F., Behrenfeld, M. J., & Boyd, P. W. (2014). Global assessment of ocean carbon export by combining satellite observations and food-web models. *Global Biogeochemical Cycles*, *28*(3), 181–196. https://doi.org/10.1002/2013GB004743

Sigman, D. M., & Hain, M. P. (2012). The Biological Productivity of the Ocean. *Nature Education Knowledge*, *3*(10): 21.

Smith, S. V. (1981). Marine macrophytes as a global carbon sink. *Science*, *211*(4484), 838–840. https://doi.org/10.1126/science.211.4484.838

Steemann Nielsen, E. (1952). The use of radio-active Carbon (C) for measuring organic production in the sea. *Fuel and Energy Abstracts*, *37*(5), 332. https://doi.org/10.1093/ICESJMS/18.2.117

Stramski, D., Reynolds, R. A., Kahru, M., & Mitchell, B. G. (1999). Estimation of particulate organic carbon in the ocean from satellite remote sensing. *Science*, *285*(5425), 239–242. https://doi.org/10.1126/science.285.5425.239

Tang, W., Li, Z., & Cassar, N. (2019). Machine learning estimates of global marine nitrogen fixation. *Journal of Geophysical Research: Biogeosciences*, *124*(3), 717–730. https://doi.org/10.1029/2018JG004828

Taylor, J. R., & Ferrari, R. (2011). Ocean fronts trigger high latitude phytoplankton blooms. *Geophysical Research Letters*, *38*(23). https://doi.org/10.1029/2011gl049312

Teeter, L., Hamme, R. C., Ianson, D., & Bianucci, L. (2018). Accurate estimation of net community production from O_2/Ar Measurements. *Global Biogeochemical Cycles*, *32*(8), 1163–1181. https://doi.org/10.1029/2017gb005874

Teira, E., José Pazó, M., Serret, P., & Fernández, E. (2001). Dissolved organic carbon production by microbial populations in the Atlantic Ocean. *Limnology & Oceanography*, *46*(6), 1370–1377. https://doi.org/10.4319/lo.2001.46.6.1370

Tobler, W. R. (1970). A computer movie simulating urban growth in the detroit region. *Economic Geography*, *46*(sup1), 234–240. https://doi.org/10.2307/143141

Tramontana, G., Jung, M., Schwalm, C. R., Ichii, K., Camps-Valls, G., Ráduly, B., et al. (2016). Predicting carbon dioxide and energy fluxes across global FLUXNET sites with regression algorithms. *Biogeosciences*, *13*(14), 4291–4313. https://doi.org/10.5194/bg-13-4291-2016

Vallina, S. M., Follows, M. J., Dutkiewicz, S., Montoya, J. M., Cermeno, P., & Loreau, M. (2014). Global relationship between phytoplankton diversity and productivity in the ocean. *Nature Communications*, *5*(4299). https://doi.org/10.1038/ncomms5299

Wanninkhof, R. (2014). Relationship between wind speed and gas exchange over the ocean revisited. *Limnology and Oceanography: Methods*, *12*(6), 351–362. https://doi.org/10.4319/lom.2014.12.351

Waring, R. H., Landsberg, J. J., & Williams, M. (1998). Net primary production of forests: A constant fraction of gross primary production? *Tree Physiology*, *18*(2), 129–134. https://doi.org/10.1093/treephys/18.2.129

Westberry, T., Behrenfeld, M. J., Siegel, D. A., & Boss, E. (2008). Carbon-based primary productivity modeling with vertically resolved photoacclimation. *Global Biogeochemical Cycles*, *22*(2), 85–85. https://doi.org/10.1029/2007gb003078

Westberry, T. K., Williams, P. J. L. B., & Behrenfeld, M. J. (2012). Global net community production and the putative net heterotrophy of the oligotrophic oceans. *Global Biogeochemical Cycles*, *26*(4), GB4019. https://doi.org/10.1029/2011GB004094

Williams, P. J. L. B., Morris, P. J., & Karl, D. M. (2004). Net community production and metabolic balance at the oligotrophic ocean site, station ALOHA. *Deep Sea Research I: Oceanographic Research Papers*, *51*(11), 1563–1578. https://doi.org/10.1016/j.dsr.2004.07.001

Zhang, Y., Song, C., Sun, G., Band, L. E., McNulty, S., Noormets, A., et al. (2016). Development of a coupled carbon and water model for estimating global gross primary productivity and evapotranspiration based on eddy flux and remote sensing data. *Agricultural and Forest Meteorology*, *223*, 116–131. https://doi.org/10.1016/j.agrformet.2016.04.003

Zhao, M., & Running, S. W. (2010). Drought-induced reduction in global terrestrial net primary production from 2000 through 2009. *Science*, *329*(5994), 940–943. https://doi.org/10.1126/science.1192666